New Physics: Sae Mulli,
Vol. 65, No. 4, April 2015, pp. 311∼316

DOI: 10.3938/NPSM.65.311

Effects of Nd-doping on the Structural, Electrical, and Multiferroic Properties of $Bi_7Fe_3Ti_3O_{21}$ Thin Films

Chinnambedu Murugesan RAGHAVAN · Jin Won KIM · Ji Ya CHOI · Sang Su KIM*
Department of Physics, Changwon National University, Changwon 641-773, Korea

(Received 3 March 2015 : revised 23 March 2015 : accepted 23 March 2015)

Aurivillius-phase six-layered $Bi_7Fe_3Ti_3O_{21}$ (BFTO21) and Nd-doped $Bi_{6.4}Nd_{0.6}Fe_3Ti_3O_{21}$ (BNdFTO21) thin films were prepared on Pt(111)/Ti/SiO_2/Si(100) substrates by using a chemical solution deposition method in order to investigate their structural, electrical, and multiferroic properties. Doping the Bi sites of the BFTO21 with Nd^{3+}-ions led to remarkable improvements in the electrical and the multiferroic properties. The electrical study of the BNdFTO21 thin film showed a low leakage current density of 4.38×10^{-6} A/cm^2 at an applied electric field of 100 kV/cm, which was about one order of magnitude lower than that of the BFTO21 thin film. The ferroelectric $P - E$ hysteresis loop of the BNdFTO21 thin film exhibited a large remnant polarization ($2P_r$) of 24 μC/cm^2 and a low coercive electric field ($2E_c$) of 154 kV/cm at an applied electric field of 239 kV/cm. Furthermore, the magnetization and the coercive magnetic field that were observed for the BNdFTO21 thin film at room temperature were drastically enhanced compared to those observed for the BFTO21 thin film.

PACS numbers: 77.84.-s
Keywords: Nd-doped $Bi_7Fe_3Ti_3O_{21}$, Chemical solution deposition, Electrical properties, Multiferroic properties

I. INTRODUCTION

The Fe-contained Aurivillius-type bismuth-layered structure compounds with ferroelectric properties (BLSF) with the general formula $Bi_{n+1}Fe_{n-3}Ti_3O_{3n+3}$ ($n \geq 4$) have recently received considerable attention because of their simple structure, lead-free nontoxic nature and the coexistence of ferroelectric and magnetic properties with a strong coupling behavior near ambient conditions [1–3]. The crystal structure of these compounds is formed by the alternating stacking of perovskite-like $(Bi_{n-1}Fe_{n-3}Ti_3O_{3n+1})^{2-}$ slabs between the fluorite-like bismuth-oxygen $(Bi_2O_2)^{2+}$ layers along the c-axis [1]. The electrical properties of these materials primarily rely on these $(Bi_2O_2)^{2+}$ layers [1, 4]. Among this family, the four-layered $Bi_5FeTi_3O_{15}$ (n = 4) and five-layered $Bi_6Fe_2Ti_3O_{18}$ (n = 5) compounds have been widely investigated both in thin film and bulk ceramic form for multiferroic and magneto-electric applications [1,2,5–9].

As an extension of this series, six-layered $Bi_7Fe_3Ti_3O_{21}$ (BFTO21) (n = 6) has recently been investigated for the multiferroic applications [3, 10–12]. The coexistence of ferroelectric and ferromagnetic properties was reported for bulk ceramics of the type BFTO21 doped with the rare earth element Gd and the transition metal Ni [11, 12]. However, in the bulk ceramic form the BFTO21 showed low ferroelectric polarization and leaky hysteresis behavior [11, 12]. For practical use in storage devices, multiferroic materials are required to exhibit a low leakage current density and well-saturated ferroelectric and magnetic hysteresis loops with a large polarization and large magnetization, respectively. Therefore, it is technologically important to improve the electrical and the multiferroic properties of the BFTO21 thin film.

In this study, thin films of the pure BFTO21 and the Nd-doped $Bi_{6.4}Nd_{0.6}Fe_3Ti_3O_{21}$ (BNdFTO21) thin films

*E-mail: sskim@changwon.ac.kr

were prepared on Pt(111)/Ti/SiO_2/Si(100) substrates by using a chemical solution deposition (CSD) method for the systematic investigations of the structural, electrical and multiferroic properties. The ionic radius of the Nd^{3+}-ion (1.109 Å) is slightly smaller than that of the Bi^{3+}-ion (1.17 Å); therefore, it is easy to incorporate into the Bi-site of the BFTO21 thin film. Furthermore, the use of the rare earth Nd^{3+}-ion for doping purposes has been strongly recommended for improving the electrical and multiferroic properties of the Fe-contained BLSF compounds [13]. However, to the best of our knowledge there are no investigations on the effect of Nd^{3+}-ion doping on the electrical and multiferroic properties of the six-layered Aurivillius BFTO21 thin film.

II. EXPERIMENTAL PROCEDURE

Thin films of BFTO21 and BNdFTO21 were deposited on Pt(111)/Ti/SiO_2/Si(100) substrates by using a CSD method. The raw materials bismuth nitrate pentahydrate, iron nitrate nonahydrate, titanium isopropoxide, and neodymium nitrate hexahydrate were used for the preparation of the precursor solutions. The solvent was prepared by mixing 2-methoxyethanol and ethylene glycol with constant stirring at room temperature. To the above solvent, acetic acid was added as a catalyst. Measured quantities of bismuth nitrate pentahydrate, neodymium nitrate hexahydrate, and iron nitrate nonahydrate were added to the above solution sequentially at 30 min intervals. A homogeneous solution of 2-methoxyethanol and acetylacetone, which was used as a stabilizing agent, was separately prepared in a glove box at room temperature, after which the titanium isopropoxide was dissolved in this mixture and stirred for 1.5 h. Finally, the Ti-solution was added to the Bi-Nd-Fe solution to form the BNdFTO21 precursor, and this solution mixture was stirred for an additional 2 h. The BFTO21 precursor solution was also prepared in the same manner for the comparison. The concentrations of the precursor solutions were calculated to be 0.1 M.

The BFTO21 and the BNdFTO21 precursor solution were deposited on the Pt(111)/Ti/SiO_2/Si(100) substrates by using a spin-coating method at an angular spin velocity of 3000 rpm for 20 s. Subsequently, the deposited wet thin films were dried and prebaked at 200 °C and 360 °C for 5 min, respectively, on a hot plate. The coating, drying, and prebaking processes were repeated 15 times to acquire the desired film thickness. Then, the thin films were annealed at 600 °C for 3 min by rapid thermal annealing under an oxygen atmosphere to achieve crystallization.

The structures of the thin films were investigated by using an X-ray diffractometer (Rigaku, MiniFlex II) and a Raman spectroscope (Jasco, NRS-3100). The surface morphologies and the film thicknesses of the thin films were examined by using a field emission scanning electron microscope (Tescan, MIRA II LMH). The platinum electrodes with areas of 1.54×10^{-4} cm^2 were deposited on the top surfaces of the thin films by ion sputtering through a metal shadow mask to measure the electrical and the ferroelectric properties. The leakage current densities of the thin films were investigated by using an electrometer (Keithley, 6517A). The ferroelectric hysteresis loops of the thin films were traced at a frequency of 1.25 kHz by using a standardized ferroelectric test system (Radiant Technologies, Precision LC). The dielectric properties were analyzed by using a low frequency impedance analyzer (HP, 4192A). The room-temperature magnetic properties of the thin films were measured by using a physical property measurement system (Quantum Design Inc., PPMS-7).

III. RESULTS AND DISCUSSION

Figure 1 shows the X-ray diffraction (XRD) patterns of the thin films deposited on Pt(111)/Ti/SiO_2/Si(100) substrates, which were obtained by interacting X-rays of wavelength 1.5418 Å generated by CuK_α. The XRD peaks of the thin films could be well indexed in accordance with the orthorhombic six-layered Aurivillius $Bi_7Fe_3Ti_3O_{21}$ structure, which has a space group of $F2mm$ [10–12]. As can be seen in Fig. 1, the BNdFTO21 thin film exhibited strong diffraction intensities compared to the BFTO21 thin film. Furthermore, the sharp (11$\underline{11}$) and the weak (22$\underline{14}$) planes were observed for the BNdFTO21 thin film, while these planes were absent from the BFTO21 thin film. These results indicated that

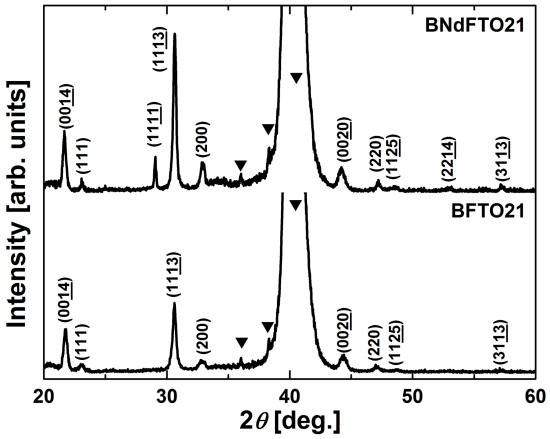

Fig. 1. XRD patterns of the BFTO21 and the BNdFTO21 thin films prepared on Pt(111)/Ti/SiO_2 /Si(100) substrates.

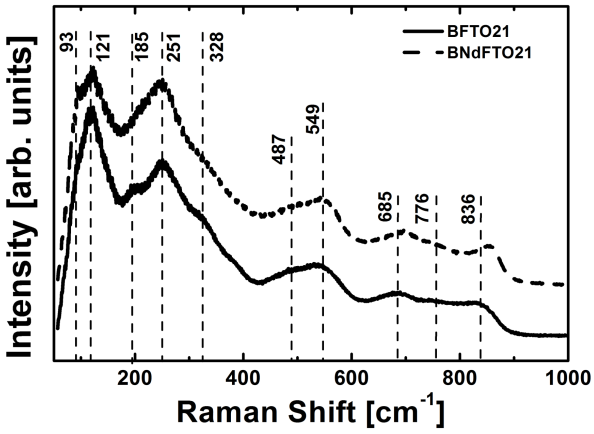

Fig. 2. Raman scattering spectra of the BFTO21 and the BNdFTO21 thin films measured at room temperature.

the crystallinity of the BNdFTO21 thin film was notably improved by doping the Bi-sites of the six-layered Aurivillius structure with Nd^{3+}-ions. It is worthy to note that there were no additional peaks corresponding to secondary or impurity phases. Moreover, there were no significant shifts in the peak positions of the BNdFTO21 thin film as compared with the BFTO21 thin film. From these results, it was inferred that the concentration of Nd^{3+}-ions that was used for doping is not sufficient to commence secondary phases or change the lattice parameters of the BNdFTO21 thin film.

The effect of Nd^{3+}-ion doping on the structure of the BFTO21 was further investigated by using a Raman scattering spectroscope. The Raman spectra of the thin films were obtained at room temperature and are shown in Fig. 2. The phonon modes of the Raman spectra of the BLSF compounds are classified into two spectral regions, which are the low frequency phonon modes (below 200 cm^{-1}) and high frequency phonon modes (above 200 cm^{-1}), respectively [14]. The phonon modes that occurred below 200 cm^{-1} are ascribed to the vibrations of Bi^{3+}-ions [14]. As shown Fig. 2, the Raman modes, which are formed at 93 cm^{-1}, 121 cm^{-1}, and 185 cm^{-1} originate from the Bi^{3+}-ion vibrations in the perovskite layer [12, 14]. The Raman modes that occurred above 200 cm^{-1} are related to the torsional bending and the stretching vibrational modes of the [Ti(Fe)O_6] octahedra [14]. The major vibrational modes, which were formed at 251 cm^{-1}, 549 cm^{-1}, and 836 cm^{-1} are ascribed to the O-Ti-O bending, Ti-O torsional bending, and Ti-O asymmetric stretching vibrations, respectively [11]. The formation of the phonon mode at 328 cm^{-1} is attributed to the ferroelectric phase transition [11]. The torsional bending mode observed at 685 cm^{-1} is assigned to the FeO_6 octahedra. The phonon mode formed at 487 cm^{-1} is assigned to the opposing extensions of the external apical oxygen atoms of the octahedra [15]. The weak mode formed at 776 cm^{-1} is related to the Ti(Fe)O_6 octahedra. As shown in Fig. 2, a broadening of the Raman bands was observed in the low frequency region, a phenomenon which could be attributed to the doping of the Nd^{3+}-ion into the Bi-site of the perovskite block [12]. A weak Raman peak was formed at 185 cm^{-1} in the BFTO21 thin film, whereas, it appeared merged as a broad peak in the BNdFTO21 thin film. Furthermore, the Raman peak at 836 cm^{-1} in the BNdFTO21 thin film was significantly stronger compared with the corresponding peak of the BFTO21 thin film. These results could be attributed to the octahedral distortion introduced into the pseudoperovskite block of the BFTO21 as a result of the presence of the Nd^{3+}-ions [12]. The Raman study is well correlated with the XRD study to confirm the formation of an orthorhombic six-layered Aurivillius structure.

The surface morphologies of the thin films were investigated by using a scanning electron microscope (SEM). Figure 3 illustrates the SEM images of the BFTO21 and the BNdFTO21 thin films deposited on Pt(111)/Ti/SiO_2/Si(100) substrates. As shown in Fig. 3, both of the thin films contain rod and platelet-like grains

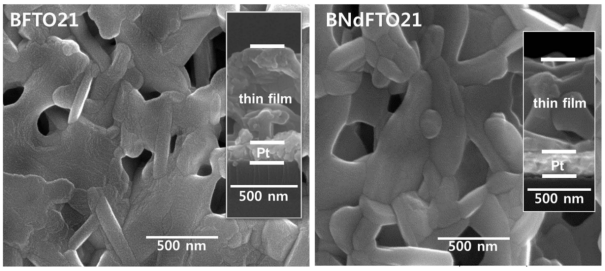

Fig. 3. Surface morphologies and cross-sectional micrographs of the BFTO21 and the BNdFTO21 thin films.

in their surface morphologies. The BFTO21 thin film exhibits wide pores resulting in a rough surface, while, the BNdFTO21 thin film showed relatively well-grown grains agglomerated on the surface. The thin films were found to have thicknesses of 630 nm (BFTO21) and 700 nm (BNdFTO21), as evaluated from the cross-sectional SEM images embedded in Fig. 3.

The plots of the leakage current densities (J) versus applied electric fields (E) of the BFTO21 and the BNdFTO21 thin films are depicted in Fig. 4. The leakage current, as shown in Fig. 4, has been suppressed by one order of magnitude as a result of doping the Bi-sites of the BFTO21 with Nd^{3+}-ions. The measured leakage current densities of the BFTO21 and the BNdFTO21 thin films were 2.43×10^{-5} A/cm^2 and 4.38×10^{-6} A/cm^2 at an applied electric field of 100 kV/cm, respectively. The large concentration of oxygen vacancies and the wide pores in the surface morphology could be attributed to the large leakage current density in the BFTO21 thin film [16]. The suppression of oxygen vacancies resulting from the doping by Nd^{3+}-ions can be related to the low leakage current density of the BNdFTO21 thin film [13]. Doping with Nd^{3+}-ions also stabilizes the perovskite structure by compensating for the Bi^{3+}-ion vacancies in the Aurivillius structure [17]. The leakage current mechanisms of the thin films were investigated by obtaining the logarithmic plots of the leakage current densities versus applied electric fields, which are shown in the inset of Fig. 4. In the inset it can be seen that both of the thin films obey Ohmic conduction mechanisms, as indicated by the linear relationship between the applied electric fields and the leakage current densities [18]. The BFTO21 and the BNdFTO21 thin films exhibited linearly fitted lines over the entire region of the applied electric field with the

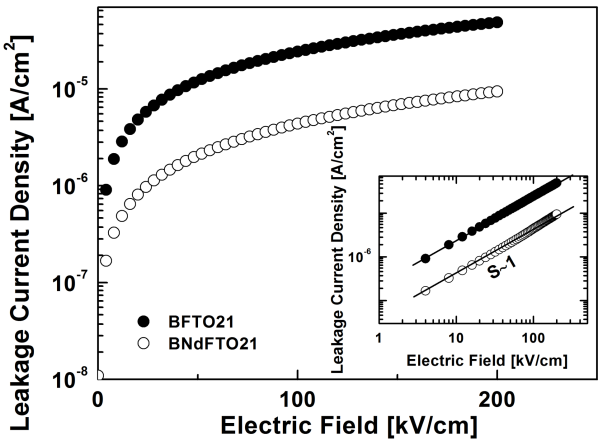

Fig. 4. Leakage current densities and $\log(J)$-$\log(E)$ characteristics of the BFTO21 and the BNdFTO21 thin films.

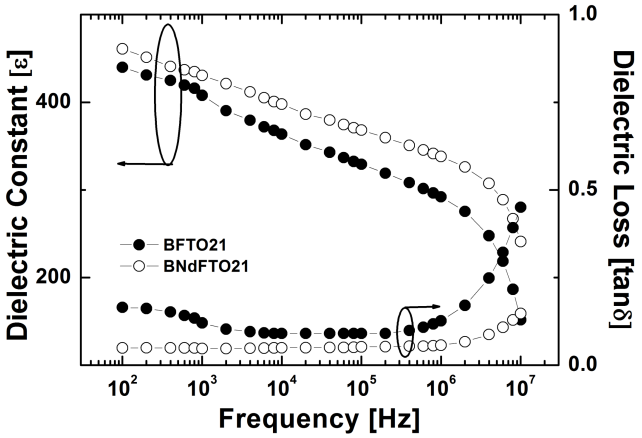

Fig. 5. Frequency-dependent dielectric properties of the BFTO21 and the BNdFTO21 thin films.

slope value S∼1, indicating that the flow of electric current in these thin films is mainly due to the thermally injected electrons [18,19]. The Ohmic conduction mechanism can be expressed as

$$J = e\mu N_e E,$$

where e is the electron charge, μ is the free carrier mobility, N_e is the density of the thermally stimulated electrons, and E is the applied electric field.

Figure 5 demonstrates the dielectric properties of the thin films measured at room temperature by varying the applied frequency in the range from 10^2 to 10^7 Hz. From Fig. 5, the measured dielectric constant (ε) and dielectric loss values for the BFTO21 and the BNdFTO21 thin films were 407 and 0.120, and 430 and 0.047, respectively, at an applied frequency of 1 kHz. This study indicates

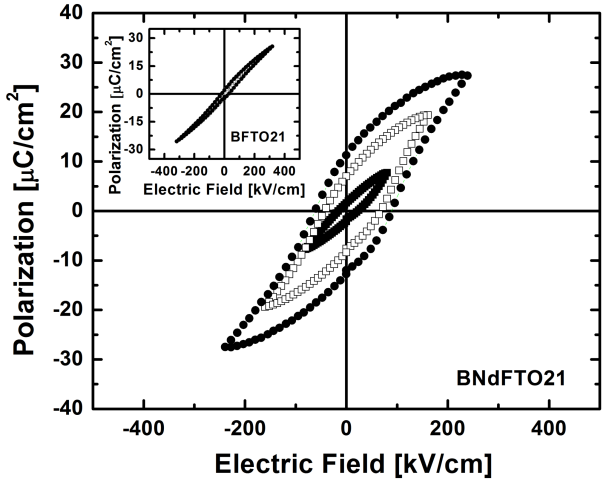

Fig. 6. Ferroelectric polarization-electric field ($P-E$) hysteresis loops of the BFTO21 and the BNdFTO21 thin films.

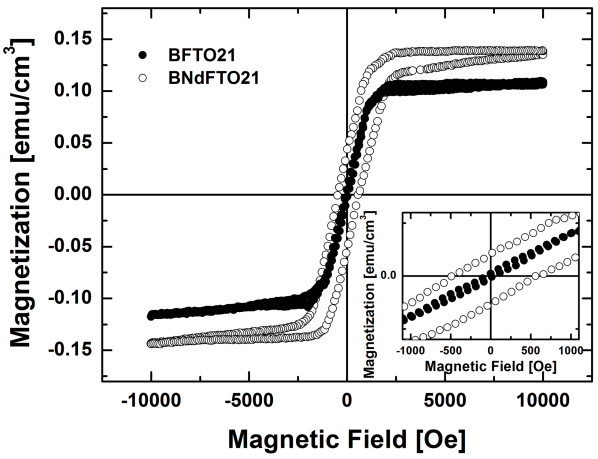

Fig. 7. Magnetization-magnetic field ($M-H$) hysteresis loops of the BFTO21 and the BNdFTO21 thin films measured at room temperature and an inset showing an enlargement of the low-field region of the $M-H$ curves to show the ferromagnetism.

that it is possible to achieve a reduction in the dielectric loss of the BNdFTO21 thin film by doping with Nd^{3+}-ions. The low value of the dielectric loss of this thin film could be well correlated to the reduced space charge contribution [20].

The effect of the Nd^{3+}-ion doping on the ferroelectric and ferromagnetic properties were investigated at room temperature. Figure 6 illustrates the ferroelectric polarization-electric field ($P-E$) hysteresis loops of the BFTO21 and the BNdFTO21 thin films, which were measured at a frequency of 1.25 kHz using triangular pulses at room temperature. As can be seen in the figure, the Nd-doped BNdFTO21 thin film exhibited well-shaped ferroelectric $P-E$ hysteresis loops with a large remnant polarization. The measured remnant polarization ($2P_r$) and coercive electric field ($2E_c$) values of the BFTO21 thin film at 318 kV/cm were 3.5 μC/cm^2 and 47 kV/cm, respectively, whereas the $2P_r$ and $2E_c$ values measured for the BNdFTO21 thin film at 239 kV/cm were 24 μC/cm^2 and 154 kV/cm, respectively. The large leakage current density could be attributed to the low polarization of the BFTO21 thin film. The suppression of the leakage current density by doping the Bi-sites of the BFTO21 with Nd^{3+}-ions could be related to the large ferroelectric polarization of the BNdFTO21 thin film [13]. The presence of a large concentration of oxygen vacancies in the ferroelectric thin films causes domain pinning, which in turn leads to poor domain switching and low ferroelectric polarization [16]. The Nd^{3+}-ion doping enhances the suppression of the oxygen vacancies; hence, it reduces domain pinning in the BNdFTO21 thin film. Furthermore, the structural distortion induced by the Nd-ion doping could also contribute to enhance the ferroelectric polarization in the BNdFTO21 thin film [13].

The magnetic field (H) dependent magnetization (M) plots of the thin films were measured at room temperature as shown in Fig. 7. The figure clearly shows that both of the thin films have well-saturated $M-H$ hysteresis loops. However, the Nd^{3+}-ion doping leads to improved ferromagnetic properties in the BNdFTO21 thin film. The inset of Fig. 7 shows enlargements of the $M-H$ plots, which were used to estimate the remnant magnetization ($2M_r$) and the coercive magnetic field ($2H_c$) values of the BFTO21 and the BNdFTO21 thin films as 0.0089 emu/cm^3 and 0.11 kOe and 0.1 emu/cm^3 and 1.04 kOe, respectively, at an applied magnetic field of 10 kOe. The enhanced magnetization of the BNdFTO21 thin film could be attributed to the structural distortion [11,12], which leads to additional tilting of the octahedra in the perovskite structure. The octahedral tilting releases locked magnetization in the dominant antiferromagnetic spiral spin state of the BFTO21 by changing the Fe^{3+}-O^{2-}-Fe^{3+} bond angle in the Aurivillius structure [12]. In overall consideration, the Nd^{3+}-ion acts as an effective dopant to improve the electrical and the multiferroic properties of the BFTO21 thin film.

IV. CONCLUSIONS

In summary, multiferroic Aurivillius phase six-layered $Bi_7Fe_3Ti_3O_{21}$ (BFTO21) and the $Bi_{6.4}Nd_{0.6}Fe_3Ti_3O_{21}$ (BNdFTO21) thin films were prepared on Pt(111)/Ti/SiO_2/Si(100) substrates by using a chemical solution deposition method. Based on the experimental results, it was inferred that Nd^{3+}-ion doping enhances the electrical and the multiferroic properties of the BFTO21 thin film. The leakage current density of the BNdFTO21 thin film was one order of magnitude lower than that of the BFTO21 thin film. Furthermore, the BNdFTO21 thin film exhibited a large ferroelectric polarization ($2P_r$) of 24 μC/cm^2 and large magnetization ($2M_r$) of 0.1 emu/cm^3 as compared with the BFTO21 thin film. The improved electrical and multiferroic properties of the BNdFTO21 thin film have been related to a decrease in the number of oxygen vacancies and the structural distortion caused by doping the Bi-site of the BFTO21 with a Nd^{3+}-ion.

ACKNOWLEDGEMENTS

This research is financially supported by Changwon National University in 2014∼2015.

REFERENCES

[1] X. Mao, W. Wang, X. Chen and Y. Lu, Appl. Phys. Lett. **95**, 082901 (2009).

[2] J. Yang, W. Tong, Z. Liu, X. B. Zhu and J. M. Dai *et al.*, Phys. Rev. B **86**, 104410 (2012).

[3] L. Keeney, T. Maity, M. Schmidt, A. Amann and N. Deepak *et al.*, J. Am. Ceram. Soc. **96**, 2339 (2013).

[4] S. K. Kim, M. Miyayama and H. Yanagida, Mater. Res. Bull. **31**, 121 (1996).

[5] H. Sun, X. Lu, T. Xu, J. Su and Y. Jin *et al.*, J. Appl. Phys. **111**, 124116 (2012).

[6] Z. Liu, J. Yang, X. W. Tang, L. H. Yin and X. B. Zhu *et al.*, Appl. Phys. Lett. **101**, 122402 (2012).

[7] C. M. Raghavan, J. W. Kim, J. Y. Choi, J. -W. Kim and S. S. Kim, Ceram. Int. **41**, 3277 (2015).

[8] X. Y. Mao, W. Wang and X. B. Chen, Solid State Commun. **147**, 186 (2008).

[9] J. Yang, L. H. Yin, Z. Liu, X. B. Zhu and W. H. Song *et al.*, Appl. Phys. Lett. **101**, 012402 (2012).

[10] A. Srinivas, M. M. Kumar, S. V. Suryanarayana and T. Bhimasankaram, Mater. Res. Bull. **34**, 989 (1999).

[11] S. Sun, Y. Ling, R. Peng, M. Liu and X. Mao *et al.*, RSC Adv. **3**, 18567 (2013).

[12] S. Sun, G. Wang, Y. Huang, J. Wang and R. Peng *et al.*, RSC Adv. **4**, 30440 (2014).

[13] F. Huang, X. Lu, C. Chen, W. Lin and X. Chen *et al.*, Solid State Commun. **150**, 1646 (2010).

[14] S. Kojima, R. Imaizumi, S. Hamazaki and M. Takashige, Jpn. J. Appl. Phys. **33**, 5559 (1994).

[15] C. Shao, Y. Lu, D. Wang and Y. Li, J. Eur. Ceram. Soc. **32**, 3781 (2012).

[16] H. Sun, J. Zhu, H. Fang and X. Chen, J. Appl. Phys. **100**, 074102 (2006).

[17] M. Li, Z. Hu, L. Pei, J. Liu and J. Wang *et al.*, Ferroelectr. **410**, 3 (2011).

[18] J. S. Kim, C. W. Ahn, H. J. Lee, S. Y. Lee and S. H. Kang *et al.*, J. Korean Phys. Soc. **46**, 147 (2005).

[19] F. -C. Chiu, H. -W. Chou and J. Y. Lee, J. Appl. Phys. **97**, 103503 (2005).

[20] I. Coondoo, A. K. Jha and S. K. Agarwal, J. Eur. Ceram. Soc. **27**, 253 (2007).